


Universal scaling of quantum state transport in a one-dimensional topological chain under nonadiabatic dynamics

Lingzi Huang,^{*} Menghua Deng,^{*} Chen Sun^{✉,†} and Fuxiang Li^{✉‡}
School of Physics and Electronics, Hunan University, Changsha 410082, China

 (Received 9 April 2024; accepted 25 June 2024; published 8 July 2024)

When a system is driven across a continuous phase transition, the density of topological defects demonstrates a power-law scaling behavior versus the quenching rate, as predicted by the Kibble-Zurek mechanism. In this study, we generalize this idea and address the scaling of quantum state transport in a one-dimensional topological system subject to a linear drive through its topological quantum phase transition point. We illustrate the power-law dependences of the quantum state's transport distance, width, and peak magnitude on the driving velocity. Crucially, the power-law exponents are distinct for the edge state and bulk state. Our results offer a different perspective on quantum state transfer and enrich the field of Kibble-Zurek behaviors and nonadiabatic quantum dynamics.

DOI: [10.1103/PhysRevB.110.014303](https://doi.org/10.1103/PhysRevB.110.014303)

I. INTRODUCTION

Quantum state transfer in quantum networks is of crucial importance in quantum control and large-scale quantum information processing [1,2]. To achieve efficient quantum state transfer across quantum networks, various transfer mechanisms have been proposed, leveraging different physical systems. Among these mechanisms, most rely on one-dimensional quantum chains with either static or dynamic parameters [3,4]. These schemes can be realized in a variety of physical systems, including photonic lattices [5–7], acoustic systems [8], nitrogen-vacancy centers in diamonds [9], superconducting qubit circuits [10,11], chains of tunnel coupled quantum dots [12], driven optical lattices [13], NMR [14], and so on.

The efficiency of quantum state transfer schemes is predominantly dictated by two main factors: the transfer speed and the fidelity [15–19]. Often, these factors are at odds, presenting a trade-off between high speed and high fidelity. While adiabatic quantum evolution can ensure perfect state transfer, it typically results in slow transfer speeds. Conversely, pursuing high transfer speeds usually incurs nonadiabatic excitations, compromising the fidelity of the quantum state [20–22]. To reconcile the two conflicting factors, the emerging field of topological states of matter provides a promising platform [23–26]. For instance, recent studies of high-fidelity quantum state transfer have utilized the Su-Schrieffer-Heeger (SSH) model to realize robust and fast quantum state transfer protocols [27–32]. The SSH model is particularly advantageous because it features edge states that are inherently resistant to external disorder owing to topological protection [33,34].

Most quantum state transfer protocols operate under adiabatic conditions, typically requiring an instantaneous energy gap to achieve high fidelity. A prominent example of this is Thouless pumping, which adiabatically transfers a quantized number of electrons over a periodic cycle [35]. It poses an intriguing question: What occurs when the system is nonadiabatically driven across a quantum critical point where the gap closes [20–22]? When a system is quenched across a continuous phase transition, topological excitations are formed, and the density of these excitations demonstrates a universal power-law scaling relationship with the quenching speed. This phenomena, known as the Kibble-Zurek mechanism (KZM) [36–41], has been experimentally verified on a variety of platforms [42–52]. Recent research expanded on the KZM, uncovering that universal characteristics are also present in the rapid quench regime, in the full counting statistics of defects and in significant fluctuations, thereby enhancing the understanding of the nonequilibrium and nonadiabatic dynamics [53–55]. This raises an interesting question: Are there more physical quantities that exhibit a scaling relationship with the quenching rate if the system traverses a critical point with a closing gap?

In this paper, we investigate the scaling behavior of quantum state transport in a one-dimensional (1D) topological chain when the system is linearly driven across the topological quantum phase transition point. We focus on the transport distance, the width, and the peak magnitude of the quantum state, revealing that each of these quantities exhibits a power-law scaling with the driving speed. Crucially, the power-law scaling exponents display distinct values for the edge state and the bulk state. We establish that our findings are applicable not only to the Hermitian SSH model but also to other 1D topological systems such as the Creutz ladder model [56,57] and non-Hermitian SSH model. Our research offers insight into the quantum state transfer and contributes to the broader understanding of Kibble-Zurek behaviors and nonadiabatic quantum dynamics.

^{*}These authors contributed equally to this work.

[†]Contact author: chensun@hnu.edu.cn

[‡]Contact author: fuxiangli@hnu.edu.cn

This paper is organized as follows. In Sec. II, we introduce the quenching protocol in an SSH model. In Sec. III, the scaling behaviors of the travel distance, the width, and the peak magnitude are discussed. In Sec. IV, we present theoretical arguments on the scaling behaviors. Sections V and VI discuss the results for the Creutz ladder model and non-Hermitian SSH model, respectively. Finally, discussion and conclusions are presented in Sec. VII. Appendixes A and B give the calculations for probabilities projected to each extended eigenstate for linear quenches from an edge and discuss the fidelity of adiabatic transfer, respectively.

II. SSH MODEL AND QUENCHING PROTOCOL

We start with the 1D SSH model to study quantum state transport under nonadiabatic dynamics when the system is driven across the topological phase transition point. Our results are also applicable to other 1D topological systems, such as the Creutz ladder model and non-Hermitian SSH model, as presented in later sections. The Hamiltonian of an open-boundary SSH chain with N unit cells reads

$$H = \sum_{n=1}^N J_1 a_n^\dagger b_n + \sum_{n=1}^{N-1} J_2 a_{n+1}^\dagger b_n + \text{H.c.}, \quad (1)$$

where a_n^\dagger (a_n) and b_n^\dagger (b_n) are the creation (annihilation) operators on the A and B sublattices in the n th unit cell. J_1 and J_2 are intracell and intercell couplings, respectively, and H.c. denotes the Hermitian conjugate of all previous terms. It is very well understood that the system undergoes a phase transition from a topologically nontrivial phase ($J_1 < J_2$) to a trivial phase ($J_1 > J_2$) with gap closing at $J_1 = J_2$.

We consider a quenching process in which an initial state $|\psi(t_i)\rangle$ evolves under the Schrödinger equation $i\frac{d}{dt}|\psi\rangle = H(t)|\psi\rangle$ to a final state $|\psi(t_f)\rangle$ with a time-dependent Hamiltonian $H(t)$. We consider two different quench protocols. The first one is called ‘‘linear quench,’’ with the couplings varying with time:

$$J_1 = \beta t, \quad J_2 = 1 - \beta t. \quad (2)$$

Quench is taken from $t_i = 0$ to $t_f = 1/\beta$, with $\beta > 0$ characterizing the speed of the quench. Such a quench connects the two fully dimerized limits $J_1 = 0, J_2 = 1$ and $J_1 = 1, J_2 = 0$. The other is called ‘‘periodic quench’’ and consists of two successive linear quenches, the quench in (2) and its mirror reflection about the $t = 1/\beta$ line, such that the system returns to the original Hamiltonian after one period and can thus be compared to a Thouless pumping process if the quenching rate β is sufficiently small.

We will consider two different initial states:

$$|\psi(t_i)\rangle = |1, A\rangle, \quad (3)$$

which is located at the left edge, and

$$|\psi(t_i)\rangle = (|n, B\rangle + |n+1, A\rangle)/\sqrt{2}, \quad (4)$$

which is located in the bulk of the chain and is far away from the edge. For example, we can choose $n = N/2$. The two initial states are both eigenstates of the initial Hamiltonian $H(t_i)$.

III. SCALING OF TRAVEL DISTANCES

We first consider the linear quench (2). In the adiabatic limit $\beta \rightarrow 0$, since the edge state is always gapped (even though it is small) from other states, $|1, A\rangle$ evolves adiabatically to the right edge state $|N, A\rangle$. In the opposite diabatic limit $\beta \rightarrow \infty$, $|1, A\rangle$ remains unchanged simply because there is no time to evolve. We are interested in the intermediate region between these two limits, where the final state is expected to be distributed over the chain. By numerically solving the time-dependent Schrödinger equation, we calculate $|\psi(t_f)\rangle$ for an open SSH chain with $N = 1000$ unit cells from an initial state at the left edge [Eq. (3)] or in the middle of the chain [Eq. (4)]. To characterize the final state, we define the final probabilities

$$p_{n,\pm} = |\langle n, \pm | \psi(t_f) \rangle|^2, \quad (5)$$

which are the probabilities of the final state projected to the final localized eigenstates $|n, \pm\rangle = (|n, A\rangle \pm |n, B\rangle)/\sqrt{2}$. Note that at the final time t_f , the Hamiltonian is dimerized, and $|n, \pm\rangle$ are its eigenstates, with energies being ± 1 . Calculations show that for $|\psi(t_i)\rangle = |1, A\rangle$ we always have $p_{n,+} = p_{n,-}$, which is due to the chiral symmetry of the system. For bulk state (4) with $n = 500$, $p_{n,-}$ is much smaller than $p_{n,+}$ due to the fact that the initial state $|\psi(t_i)\rangle$ is an eigenstate of the initial Hamiltonian with a positive eigenvalue. Thus, it suffices to focus on $p_{n,+}$. One sees qualitatively different behaviors for the two types of initial states: For evolutions from the edge [Fig. 1(a)], $p_{n,+}$ shows a smooth profile with a single peak, resembling a coherent state, whereas for evolutions from the middle [Fig. 1(b)], $p_{n,+}$ develops oscillations whose strength increases when moving away from the initial position until a peak emerges, followed by a sharp falloff to zero at large n . We also note that, as depicted in Fig. 1(c), the transport does not start until near the critical point at time $t = 0.5/\beta$. This observation will be helpful for understanding the scaling behaviors later.

The scaling behaviors of the initial edge state are summarized in Fig. 1(d), in which the probability distributions $p_{n,+}$ for different values of the quenching rate β collapse to a single curve after one rescales n and $p_{n,+}$ by β . This indicates that all the quantities, such as the travel distance and peak magnitude, that are related to the transported quantum state will exhibit power-law relations with the quenching rate, as illustrated in Fig. 2. First, we consider how far the state travels under the quench. We define the position of the peak as the traveled distance d . In Fig. 2(a), d exhibits a power-law scaling for both the initial edge state and bulk state $d \propto \beta^{-\nu}$, but with different scaling exponents. For the edge state, $\nu \approx 0.61$, while for the bulk state, $\nu \approx 1.03$. For the initial edge state, one can also study the width of the profile of $p_{n,+}$, defined by the standard variance $w_{\text{edge}} = [\sum_n (n-d)^2 p_{n,+}]^{1/2}$. As plotted in Fig. 2(b), it also exhibits a power-law scaling with the same exponent as the travel distance: $w_{\text{edge}} \propto \beta^{-0.61}$.

Moreover, in Fig. 2(c) the maxima of the probability distribution $p_{n,+}$ of both the initial edge state and initial bulk state are plotted as a function of the quenching rate β . We see that again, the maximum exhibits a power-law scaling with β , but with different scaling exponents for the two types of initial states. For the initial edge state, the exponent is roughly 0.61,

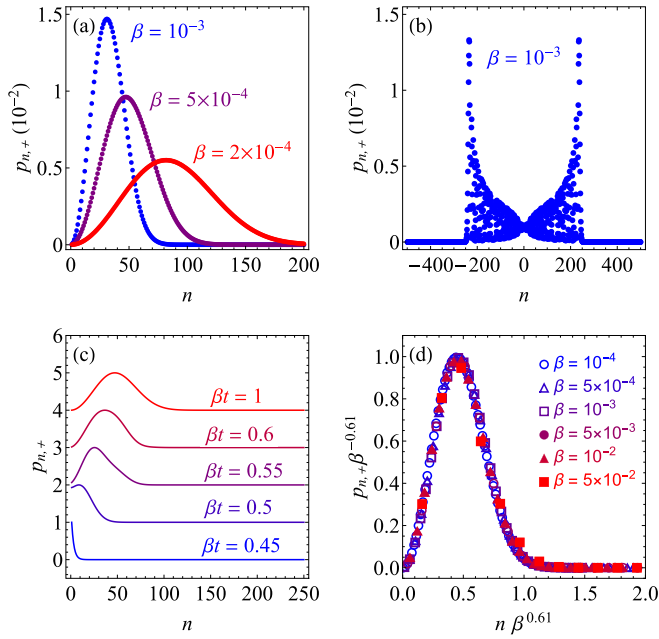


FIG. 1. Distribution of probabilities $p_{n,+}$ vs n for different initial states. (a) and (b) are the distributions of the final probabilities for initial edge state (3) and for bulk state (4), respectively. In (b) the n axis is shifted such that the initial bulk state is at $n = 0$. (c) Probability profiles $p_{n,+}$ at different times for a fixed quenching rate $\beta = 5 \times 10^{-4}$. Each profile is stretched vertically so the maximum $p_{n,+}$ becomes 1. (d) The probability profiles $p_{n,+}$ of the initial edge state for different values of β collapse to a single curve after scaling of n and $p_{n,+}$.

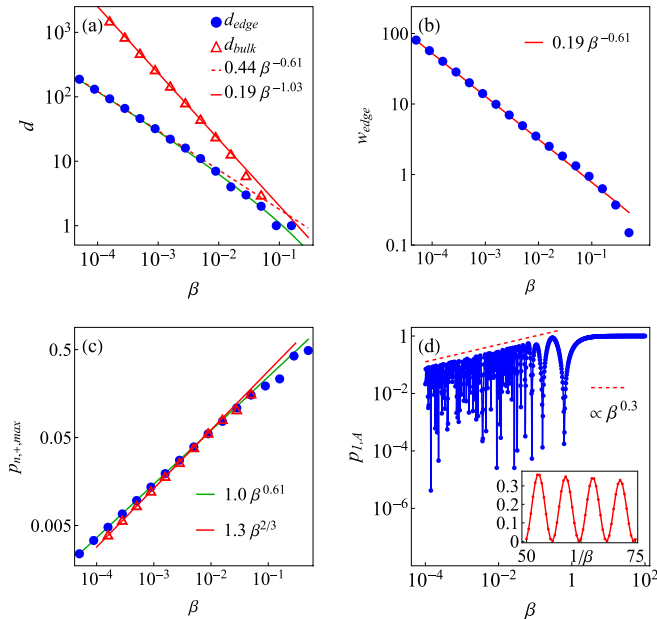


FIG. 2. Scalings in the open SSH chain for $N = 1000$: (a) scaling of the travel distance, (b) scaling of the width, (c) scaling of $p_{n,+}$ at the peak. Numerical results are represented by blue dots for the initial edge and red triangles for the initial bulk state. Solid lines are power-law fittings. (d) Probability $p_{1,A}$ to return to the edge for a periodic quench from an initial edge state. The inset shows that $p_{1,A}$ oscillates with a period $2\pi/\beta$.

while for the initial bulk state, $2/3$ fits the numerical results very well.

We note that in all our calculations $p_{n,+}$ decay fast to zero for n sufficiently far away from the initial positions. We find that under periodic boundary conditions, the results for evolutions from the bulk also fulfill the same scalings, $d_{\text{PBC}} \propto \beta^{-1.03}$ and $p_{n,+,\text{max}} \propto \beta^{2/3}$. We note that different boundary conditions or different lengths of the lattice do not change these results as long as the end of the chain is not reached by the state evolution.

For periodic quench, after one periodic circle, one would expect that the state would transfer from one edge state to another edge state located at the other end of the chain if the quench is slow enough that the system is in the adiabatic regime, which is called Thouless pumping. However, when crossing a topological phase transition point with gap closing, near this gap-closing point the adiabatic condition always breaks no matter how slow the quench is; this follows from the adiabatic theorem, which states that the conditions of an adiabatic evolution are that the quench is slow enough and that the spectrum of the system is always gapped. Thus, the adiabatic condition cannot be fully satisfied, leading to nonzero populations of excited states, and thus, the quantized state transfer cannot be realized. Here, in order to quantify the state transfer, we examine the final probability at the first lattice point $p_{1,A}$ after one periodic quench. Plotting $p_{1,A}$ vs β for quenches from an edge in Fig. 2(d), we see that $p_{1,A}$ oscillates between zero and an upper bound $p_{1,A,\text{max}}$, which scales as $\beta^{0.3}$. Plotting $p_{1,A}$ vs $1/\beta$ shows that this oscillation has a fixed period of $2\pi/\beta$ [inset of Fig. 2(d)].

It is interesting to see whether the observed scaling laws apply to other quench protocols. For evolution from an edge, we considered a quench with a sinusoidal shape,

$$J_1 = \sin^2(\beta t), \quad J_2 = \cos^2(\beta t) \quad (6)$$

from $t_i = 0$ to $t_f = \pi/(2\beta)$. We find that the behavior of $p_{n,+}$ is similar to the linear quench shown in Fig. 1.

For evolution from the bulk, we considered the above sinusoidal quench and a sudden quench where J_1 and J_2 are both set to nonzero constants from $t = 0$ to $t_f = 1/\beta$ and found the same scaling laws, $d_{\text{bulk}} \propto \beta^{-1}$ and $p_{n,+,\text{max}} \propto \beta^{2/3}$.

IV. THEORY OF QUENCHES

In this section, we present theoretical arguments on the scaling behaviors of the quantum state transport under the nonadiabatic quench dynamics discussed above.

A. Theory of quench from an edge

To understand the scaling behaviors, we first look at the spectrum of the system. For a chain with an odd number of sites, the eigenvalues of the Hamiltonian have analytical forms [58]: There is a single edge state with zero energy, and $2N - 2$ extended states with energies

$$E = \pm \epsilon_j = \pm |J_2 + J_1 e^{ik_j}|,$$

where $k_j = \pi j/N$ and $j = 1, 2, \dots, N - 1$. As a result of this spectrum, during an evolution the edge state is gapped from all the extended states except near time $t = t_f/2 = 1/(2\beta)$. For

an evolution starting from the left edge, we expect that during the quench the state should remain near the left edge until close to $t_f/2$, when the gaps become minimal [see Fig. 1(c)]. At $t_f/2$, a portion of the state transfers to each extended state, which then travels at the group velocity of the extended state

$$v_k = d\epsilon_j/dk = J_1 J_2 \sin(k_j)/\epsilon_j, \quad (7)$$

and the whole state is a superposition of the traveling of each extended state. In Appendix A, we further justify this picture by calculating probabilities projected to each extended eigenstate.

Based on this picture, we can estimate the travel distance d_{edge} . Note that the Hamiltonian depends linearly on time and thus constitutes a multilevel Landau-Zener (LZ) problem, which may not be solved exactly. The traditional LZ problem is to find the transition probabilities from an initial state to each final energy state. The exactly solvable models are rare and have been found to exist only in some special forms [59–63]. Here, instead of looking for an exact solution, we provide an ansatz that can be fitted by numerical results. We observe that the transition probability to each final state (denoted as p_k [64]) is solely determined by a dimensionless parameter Δ_k^2/β , where $\Delta_k = \epsilon_k = \cos(k/2)$ is the gap between an extended state and the edge state at $t = t_f/2$. One can use the following ansatz:

$$p_k = c_3 \left(1 - e^{-\frac{c_1 \Delta_k^2}{\beta}}\right) e^{-\frac{c_2 \Delta_k^2}{\beta}}. \quad (8)$$

c_1 and c_2 are two fitting parameters, and c_3 is an overall normalization factor. A comparison with numerical results is presented in Appendix A. Note that p_k is small for both small and large Δ_k , and it reaches a peak at $\Delta_k^2/\beta \approx 1$. The wave vector corresponding to this peak is $k = 2 \arccos \sqrt{\beta}$, which can be used to estimate the travel distance as

$$d_{\text{edge}} = \int_{1/(2\beta)}^{1/\beta} |v_k| dt, \quad (9)$$

assuming that the traveling starts roughly at time $1/(2\beta)$ and ends at time $1/\beta$. This integral can be analytically performed, giving

$$d_{\text{edge}} = \frac{1}{8\sqrt{\beta}} \left(\frac{2-\beta}{1-\beta} \operatorname{arccosh} \frac{1}{\sqrt{\beta}} - \sqrt{\frac{1}{1-\beta}} \right). \quad (10)$$

The green curve in Fig. 2(a) is Eq. (10), which agrees well with the exact d_{edge} , and for large β it correctly predicts the drop in d_{edge} below the power-law scaling.

The power-law scaling of d_{edge} can now be understood. Since $\beta \ll 1$ in almost the whole range of β considered, keeping the leading order in β gives

$$d_{\text{edge}} \approx \frac{1}{8\sqrt{\beta}} \left(\ln \frac{4}{\beta} - 1 \right). \quad (11)$$

Thus, d_{edge} scales as $d_{\text{edge}} \propto \beta^{-1/2} \ln(1/\beta)$, which is visually close to a power law $d_{\text{edge}} \propto \beta^{-\nu}$ with some $\nu > 1/2$ within a range of β .

B. Theory for quench from the bulk

As mentioned before, for evolution from the bulk we can consider a chain with periodic boundaries. Now the Hamiltonian can be reduced to a 2×2 matrix in the momentum space labeled by $k = 2\pi j/N$ ($j = 0, 1, \dots, N-1$), with eigenenergies $E = \pm\epsilon_k = \pm|J_1 + J_2 e^{-ik}|$. Let us denote the corresponding eigenvectors in the k th block as $|\psi_{k,\pm}\rangle$. The initial localized state $|\psi(t_i)\rangle = (|n_i, B\rangle + |n_i + 1, A\rangle)/\sqrt{2}$ can be written as a superposition of all eigenstates with positive energies:

$$|\psi(t_i)\rangle = (1/\sqrt{N}) \sum_k e^{-ikn_i} |k\rangle \otimes |\psi_{k,+}\rangle. \quad (12)$$

During the quench each $|k\rangle \otimes |\psi_{k,+}\rangle$ travels with velocity $v_k = \partial\epsilon_j/\partial k$ and reaches a distance $\int_0^{1/\beta} v_k dt$ at the final time [65]. Note that unlike evolution from the edge, the traveling starts immediately at $t = 0$. We can estimate the travel distance d_{bulk} as the largest distance traveled by all the eigenstates, which simply gives rise to $d_{\text{bulk}} = c/\beta$ obtained with a change in the variable $t \rightarrow t/\beta$. Here, c is a constant and is numerically determined to be around 0.24.

To understand the magnitude of the peak $p_{n,+,\max}$, we consider the corresponding amplitude, which can be approximated by assuming adiabatic evolution [66]:

$$\langle n_{\max,+} | \psi(t_f) \rangle = (1/N) \sum_k e^{-ikn_i} e^{i(kn_{\max} - \varphi_k)}, \quad (13)$$

where $\varphi_k = \int_0^{1/\beta} \epsilon_k dt$ is the adiabatic phase accumulated during the evolution of $|\psi_{k,+}\rangle$. The magnitude can be estimated by the stationary phase approximation. Let us consider Taylor expansion of φ_k near k_{\max} , which is the momentum labeling each final state with maximum transition probability. Therefore, we have $(\partial^2 \varphi_k / \partial k^2)_{k_{\max}} = 0$. Since $\partial\varphi_k/\partial k = \int_0^{1/\beta} v_k t dt$, we have $(\partial\varphi_k/\partial k)_{k_{\max}} = d_{\text{bulk}} = n_{\max} - n_i$. Thus, the exponent in $\langle n_{\max,+} | \psi(t_f) \rangle$ is dominated by the third-order expansion $(k - k_{\max})^3$ term. It is easy to see that $\varphi_k \propto 1/\beta$, so $(\partial^3 \varphi_k / \partial k^3)_{k=k_{\max}} = C/\beta$, where C is a constant. Replacing the summation \sum_k by integration $\int dk/(2\pi/N)$, we arrive at

$$\langle n_{\max,+} | \psi(t_f) \rangle \approx \frac{1}{2\pi} \int_{-\infty}^{\infty} dk e^{-i(\frac{C}{6\beta})(k-k_{\max})^3}, \quad (14)$$

which scales as $\propto \beta^{1/3}$, and thus, $p_{n,+,\max} = |\langle n_{\max,+} | \psi(t_f) \rangle|^2 \propto \beta^{2/3}$.

C. Theory of periodic quench

We now consider the probability $p_{1,A}$ to return to the left edge in a periodic quench, which can be considered as consisting of two linear quenches. The return probability is given by $p_{1,A} = |\sum_k (A_{k,+} + A_{k,-})|^2$, where $A_{k,\pm}$ is the amplitude contributed by an extended state labeled by k and \pm . It can be written as $A_{k,\pm} = \sqrt{p'_k} \sqrt{p'_k} e^{-i\varphi_{k,\pm}}$, where p'_k is the transition probability from the extended state to the edge state during the second linear quench, and $\varphi_{k,\pm}$ is the phase for this amplitude. The sum in $p_{1,A}$ can be simplified by noticing that the multistate LZ model corresponding to the considered linear quench belongs to bipartite models studied in [61]. According to [61], the transition probability matrix of such a model is symmetric, so $p'_k = p_k$. Moreover, chiral symmetry further

implies $\varphi_{k,+} = -\varphi_{k,-}$. Thus, we have

$$p_{1,A} = \left(2 \sum_k p_k \cos \varphi_{k,+} \right)^2. \quad (15)$$

We may approximate $\varphi_{k,+}$ at $k \sim \pi$ by the adiabatic phase accumulated during the quench, namely, the area under the curve of ϵ_k in an E vs t diagram. Since the peak of p_k is at $k = 2 \arccos \sqrt{\beta}$, which for $\beta \ll 1$ is close to π , we need to calculate only $\varphi_{k,+}$ for $k \sim \pi$, which is simply $\varphi_{k,+} \approx \int_{1/(2\beta)}^{3/(2\beta)} \epsilon_k dt = 1/(2\beta)$. Therefore, we arrive at the observed result that $p_{1,A}$ oscillates with a period of $2\pi/\beta$. In fact, what takes place here is the phenomenon of Landau-Zener-Stückelberg interferometry [67]: The interference between the total amplitude of all positive-energy extended states $\sum_k A_{k,+}$ and that of all negative-energy extended states $\sum_k A_{k,-}$ leads to a periodic dependence of the return probability on $1/\beta$. A maximum is reached whenever $\sum_k A_{k,+}$ and $\sum_k A_{k,-}$ are in constructive interference, namely, when $\arg(\sum_k A_{k,+}) = 0$. Thus, at a given β the upper bound of $p_{1,A}$ reads $p_{1,A,\max} = |2 \sum_k p_k e^{i\varphi_{k,+}}|^2$. The calculation of $p_{1,A,\max}$ using Eq. (15) with numerically obtained p_k and $\varphi_{k,+}$ agrees well with the upper bound of $p_{1,A}$ in Fig. 2(d).

V. SCALING BEHAVIORS IN THE CREUTZ LADDER MODEL

We have considered the SSH model as an example to study the scaling behaviors of quantum state transfer under nonadiabatic quench dynamics. To illustrate that the scaling behavior is not restricted to some special model but is universal, we now consider another model originally proposed by Creutz in [56]. The Creutz model is also a 1D chain consisting of two lattice points, A and B , as depicted in Fig. 3. The Hamiltonian reads

$$\begin{aligned} H_{\text{Creutz}} = & - \sum_{i=1}^N [K(a_n^\dagger b_{n+1} + b_n^\dagger a_{n+1}) \\ & + K(e^{-i\theta} a_n^\dagger a_{n+1} + e^{i\theta} b_n^\dagger b_{n+1}) \\ & + M a_n^\dagger b_n + \text{H.c.}], \end{aligned} \quad (16)$$

where n labels unit cells with a total of N ; A and B label the sublattices; and M , K , and $Ke^{-i\theta}$ are the vertical, diagonal, and horizontal hopping integrals, respectively. The phase factor $e^{\pm i\theta}$ mimics the presence of a magnetic field which pierces the ladder and supplies a magnetic flux θ/π per plaquette. a_n^\dagger (a_n) and b_n^\dagger (b_n) are the creation (annihilation) operators on sublattices A and B in the n th unit cell, respectively. We consider two different quenching protocols. The first one is quenching M and K ,

$$M = \beta t, \quad K = 1 - \beta t, \quad (17)$$

with fixed $\theta = -\pi/2$ and time changing from $t_i = 0$ to $t_f = 1/\beta$. The second one is quenching θ in the following way:

$$\theta = \beta t - \pi/2 \in \left(-\frac{\pi}{2}, \frac{\pi}{2}\right), \quad (18)$$

with fixed $M = 0$ and $K = 1$ and time changing from $t_i = 0$ to $t_f = \pi/\beta$. Both of the quench protocols are described by

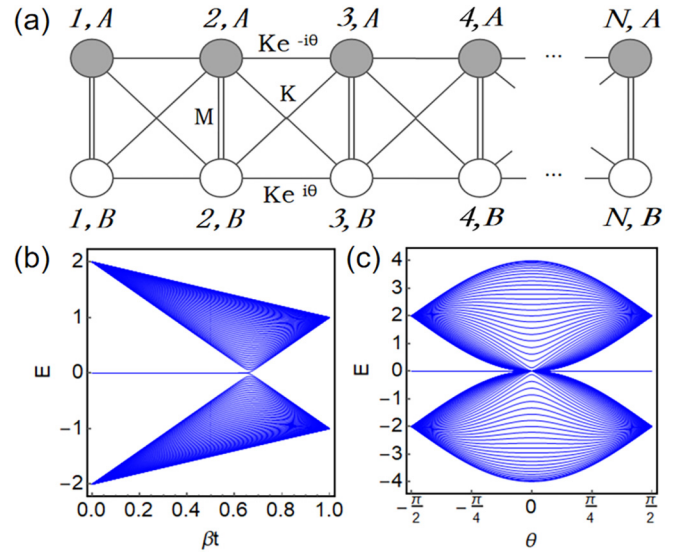


FIG. 3. (a) Diagram depicting the structure of the Creutz ladder model, with A and B being the two sublattices. W , K , and $Ke^{\pm i\theta}$ are the vertical, horizontal, and diagonal hopping integrals. (b) The spectrum of E vs βt for quenching M and K of the Creutz ladder model. (c) The spectrum of E vs βt for quenching the complex phase θ of the Creutz ladder model.

the quenching rate β . The instantaneous eigenvalues of the Hamiltonian as a function of time t are plotted in Fig. 3.

We consider two different initial localized states. One is a plaquette-blocked state,

$$|\psi(t_i)\rangle_n = \frac{1}{2}(-ia_n^\dagger + b_n^\dagger + a_{n+1}^\dagger - ib_{n+1}^\dagger)|0\rangle, \quad (19)$$

localized in the middle of the chain with $n = N/2$. The other is a topological edge state located at the left edge:

$$|L\rangle = \frac{1}{\sqrt{2}}(a_1^\dagger - ib_1^\dagger)|0\rangle. \quad (20)$$

Note that these initial states are eigenstates of the initial Hamiltonian.

The two quenching protocols start with the same initial parameters but go through different phases. Under open boundary conditions, the initial parameters are $M = 0, K = 1$, and $\theta = -\pi/2$; there are two localized chiral zero-energy modes at the left edge and the right edge. For the first quench protocol quenching M and K , the system undergoes a phase transition at time $t = 0.65/\beta$, after which the system enters a topologically trivial phase with no edge states [as shown in Fig. 3(b)]. For the second quench protocol in which only θ is quenched, we can see that there are always two zero-energy modes, as shown in Fig. 3(c), even though the system crosses a quantum critical point at $\theta_c = 0$ with gap closing.

We now discuss the scaling behavior of quantum state transfer under the quench dynamics of the Creutz ladder model by numerically solving the time-dependent Schrödinger equation for a chain with $N = 1000$. First, we study the first quench protocol that quenches M and K . We plot the probability profile p_n of the final state in Fig. 4(a) for the two different initial states, the left edge state $|L\rangle$ and the plaquette-block state $|\psi(t_i)\rangle_{n,+}$ localized in the middle of

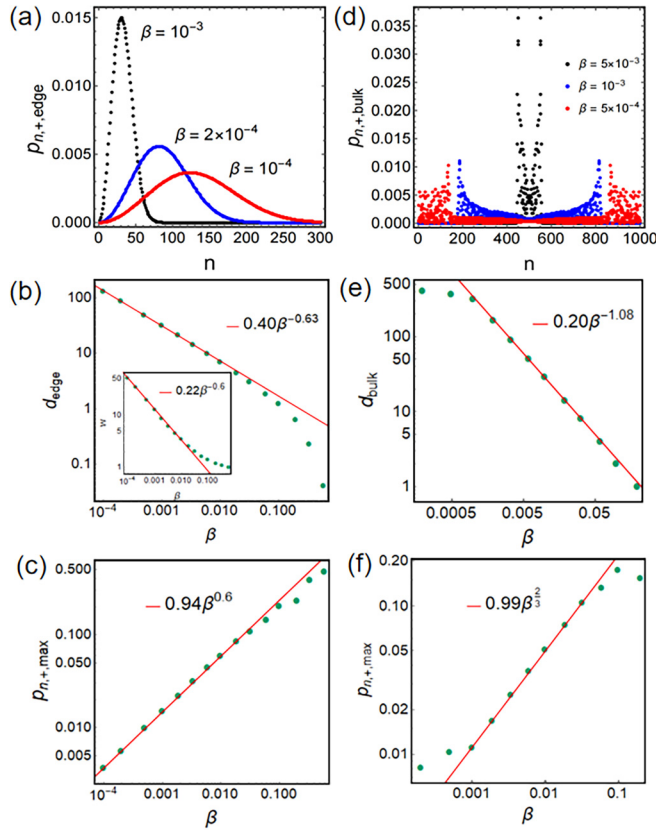


FIG. 4. Profile of $p_{n,+}$ and scalings of quenching M and K in the open Creutz ladder for $N = 1000$ for different initial states: (a)–(c) left edge state $|L\rangle$ and (d)–(f) bulk platform $|\psi(t_i)\rangle_n$. (a) and (d) are distribution diagrams for two cases at different β distinguished by black, blue, and red dots. Scalings of travel distances and the maximum of $p_{n,+}$ for $|L\rangle$ provided in (b) and (c) show $d_{\text{edge}} \propto \beta^{-0.63}$ and $p_{n,+,\text{max}} \propto \beta^{0.6}$. (e) and (h) show that the bulk platform state transmits at the scaling as $d \propto \beta^{-1.08}$ and $p_{n,+,\text{max}} \propto \beta^{\frac{2}{3}}$.

the chain with $n = 500$. Like in the case of the SSH model, we can see that the distribution of final states exhibits quite different profiles for the two different initial states. For the initial edge state, the final state has a smooth profile for different values of β , while for the initial plaquette-block state, the shape of the final state is not smooth but, instead, shows two sharp peaks.

Further, we study the scaling of the travel distances d and the maximum of $p_{n,+}$ as a function of the quenching rate β . Compared with the result in the SSH model, for quenching from the edge state, the travel distance and the maximum of $p_{n,+}$ obey almost the same power-law scaling, with $d_{\text{edge}} \propto \beta^{-0.63}$ and $p_{n,+,\text{max}} \propto \beta^{0.6}$. Additionally, the scalings for evolution from $|\psi(t_i)\rangle_n$ are almost in accordance with that in the case of evolution from the SSH middle state, which has $d_{\text{bulk platform}} \propto \beta^{-1.08}$ and $p_{n,+,\text{max}} \propto \beta^{\frac{2}{3}}$.

For the second quench protocol, unfortunately, if the initial state is on the edge, e.g., $|L\rangle$, the state does not move and is always localized in the original location. For the initial plaquette-block state, we obtain the same scaling exponents for the distance and peak of the transported wave function.

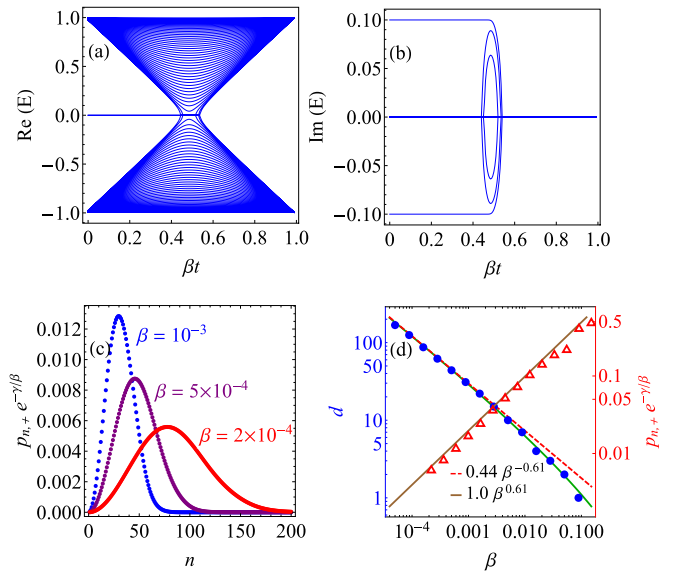


FIG. 5. Energy spectrum of a non-Hermitian SSH model and the scaling behavior of the traveled quantum state. (a) The real part and (b) imaginary part of the instantaneous energy levels as a function of time. (c) Rescaled probability profile for different values of the quench rate β . (d) Scalings of traveled distances and the maximum of $p_{n,+}$ for the initial edge state. The numbers of unit cells is taken as $N = 50$ for (a) and (b) and $N = 500$ for (c) and (d).

VI. SCALING BEHAVIOR OF THE NON-HERMITIAN SSH MODEL

We consider a non-Hermitian SSH model with imaginary on-site energy $i\gamma$ and $-i\gamma$:

$$H = \sum_{n=1}^N [(J_1 a_n^\dagger b_n + J_2 a_{n+1}^\dagger b_n + \text{H.c.}) + i\gamma a_n^\dagger a_n - i\gamma b_n^\dagger b_n]. \quad (21)$$

Here, we still quench J_1 and J_2 in such a protocol:

$$J_1 = \beta t, \quad J_2 = 1 - \beta t \quad (22)$$

from time $t_i = 0$ to $t_f = 1/\beta$, with β being the quenching rate. Even in the presence of imaginary on-site energy, at the initial time, the system is dimerized, with two edge states located at the two ends of the chain. At the final time t_f , the system is also dimerized, with eigenenergies $\varepsilon_{\pm} = \pm\sqrt{1 - \gamma^2}$ and eigenstates

$$|\pm\rangle = \frac{1}{\sqrt{2}} [|n, A\rangle + (\pm\sqrt{1 - \gamma^2} - i\gamma) |n, B\rangle]. \quad (23)$$

During the quench, the system undergoes two exceptional points at $J_1 - J_2 = \pm\gamma$. The instantaneous eigenenergies with open boundary conditions are plotted in Figs. 5(a) and 5(b). The probability distributions $p_{n,+}$ for the initial edge state after linear quench dynamics are numerically calculated for different values of the quench rate β . The profile is similar to that in the Hermitian case, but with a very large magnitude of the order of $e^{\gamma/\beta}$ due to the non-Hermitian term. Nevertheless, after rescaling the probability with a factor $e^{-\gamma/\beta}$, we can still obtain a very well defined probability profile, as shown

in Fig. 5(c) for different values of β . Like in the Hermitian SSH model and Creutz ladder model, we still have scaling behaviors for the travel distance d and peak magnitude $p_{n,+,\max}$, with the latter rescaled by $e^{-\gamma/\beta}$. The scaling exponent is the same, 0.61, which indicates a universal value.

VII. DISCUSSION AND CONCLUSIONS

We considered the dynamical behaviors of quantum state transport in a 1D topological chain which is driven across the topological phase transition with gap closing. We found that the state transport exhibits universal power-law scaling behaviors with the quenching rate, which enriches the Kibble-Zurek phenomena. More importantly, starting from the edge state or bulk state will produce distinct scaling exponents. After a periodic quench circle, Thouless pumping does not hold if the topological transition is crossed; rather, the probability of returning to the initial edge state is nonzero and also exhibits power-law scaling with the quenching rate. Our results are of broad interest in nonequilibrium quantum statistical mechanics, connecting quantum state transfer with the breakdown of adiabatic dynamics, and should find broad applications in quantum information, quantum annealing, ultracold atom physics, and the study of critical phenomena.

ACKNOWLEDGMENTS

This paper was supported by the National Key Research and Development Program of the Ministry of Science and Technology (Grant No. 2021YFA1200700), the National Natural Science Foundation of China (Grants No. 12275075, and No. 12105094), and the Fundamental Research Funds for the Central Universities of China.

APPENDIX A: PROBABILITIES PROJECTED TO EXTENDED EIGENSTATES FOR LINEAR QUENCHES FROM AN EDGE

In the main text, for linear quenches from the edge, our theoretical estimate of the travel distance is based on the picture that the edge state transfers to each extended state near $t = t_f/2$, which then travels at its group velocity. Here, we justify this picture by calculating the probabilities projected to each extended eigenstate.

We work on a chain with an odd number of sites whose eigenvalues and eigenstates have analytical forms. The eigenvalues, from lowest to highest (assuming that J_1 and J_2 have the same sign), are [58]

$$\begin{aligned} \epsilon_j &= -|J_1 + J_2 e^{-ik_j}| \quad \text{for } j = 1, 2, \dots, N-1, \\ \epsilon_N &= 0, \\ \epsilon_j &= |J_1 + J_2 e^{-ik_j}| \quad \text{for } j = N+1, \dots, 2N-1, \end{aligned} \quad (\text{A1})$$

where $k_j = \pi j/N$. (Note that, unlike in the main text, we used the integer j to label the states, which now range from 1 to $2N-1$. The definition of ϵ_j is also different from ϵ_k ; it

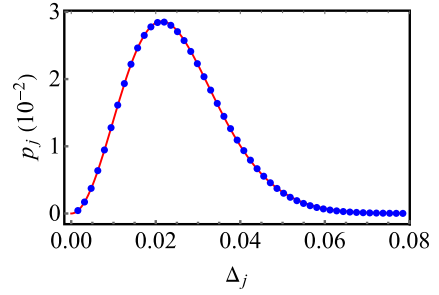


FIG. 6. p_j vs Δ_j at $\beta = 5 \times 10^{-4}$ for $N = 1000$ sites for evolutions from an edge. The blue dots are exact results, and the red line is a fitting by Eq. (A5) with $c_1 = 1.03$, $c_2 = 0.657$, and $c_3 = 0.0856$.

can now take negative values.) The corresponding normalized eigenstates are

$$|\psi_j\rangle = \frac{1}{\sqrt{N}} \left[- \sum_{n=1}^N \sin(nk_j + \phi_j) |n, A\rangle + \sum_{n=1}^{N-1} \sin(nk_j) |n, B\rangle \right] \quad \text{for } j < N, \quad (\text{A2})$$

$$|\psi_N\rangle = \sqrt{\frac{1 - (J_1/J_2)^2}{1 - (J_1/J_2)^{2N}}} \sum_{n=1}^N \left(-\frac{J_1}{J_2} \right)^{n-1} |n, A\rangle, \quad (\text{A3})$$

$$|\psi_j\rangle = \frac{1}{\sqrt{N}} \left[\sum_{n=1}^N \sin(nk_j + \phi_j) |n, A\rangle + \sum_{n=1}^{N-1} \sin(nk_j) |n, B\rangle \right] \quad \text{for } j > N, \quad (\text{A4})$$

where $\phi_j = \arg(J_1 + J_2 e^{-ik_j})$ is a phase shift on sublattice A. $|\psi_N\rangle$ is the edge state, which is localized at the left (right) end of the chain if $J_1 < J_2$ ($J_1 > J_2$). All other eigenstates are extended; note that they depend on time through ϕ_j .

With these analytical expressions, one can readily calculate $|\langle \psi_j | \psi(t) \rangle|^2$, i.e., probabilities of the evolving state projected to each extended eigenstate at any time. We looked at $|\langle \psi_j | \psi(t) \rangle|^2$ at the final time t_f of a linear quench, which we denote as p_j . We observe that $p_j = p_{2N-j}$, which originates from chiral symmetry, so it suffices to consider only the $j > N$ states. Figure 6 shows p_j vs Δ_j [$\Delta_j = |\cos(k_j/2)|$ is the gap between the j th extended state and the edge state at $t = t_f/2$] at $\beta = 5 \times 10^{-4}$. We see that as Δ_j increases, p_j increases from zero, reaches a peak, and then decreases to zero. We find that for different β the profiles of p_j vs Δ_j can be fitted by a function of the form

$$p_j = c_3 \left(1 - e^{-\frac{c_1 \Delta_j^2}{\beta}} \right) e^{-\frac{c_2 \Delta_j^2}{\beta}}. \quad (\text{A5})$$

The fitting parameters c_1 and c_2 depend slightly on β , and c_3 is an overall normalization factor. At $\beta = 5 \times 10^{-4}$, p_j reaches its maximum at $\Delta_j^2/\beta = 0.967$.

We further use p_j to calculate the final state's profile $p_{n,+}$ by assuming that the j th eigenstate travels at a speed $|v_k| = |\partial \epsilon_j / \partial k|$ and finally produces a wave package with a strength p_j centered at $d_j = \int_{1/(2\beta)}^{1/\beta} |v_k| dt$, and the final profile $p_{n,+}$ is a summation of all these wave packages. Each wave package

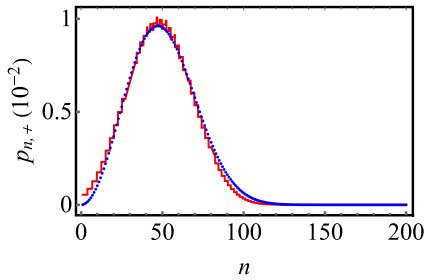


FIG. 7. $p_{n,+}$ vs n at $\beta = 5 \times 10^{-4}$ for $N = 1000$ sites for evolutions from an edge. The blue dots are exact results, and the red line is from the calculation using p_j as described in the text, with each wave package taken as a rectangular function $(p_j/40)\text{rect}[(n-1-d_j)/40]$.

has a certain shape with a certain width which our theory does not predict, and we simply take it to be the rectangular function $(p_j/W)\text{rect}[(n-1-d_j)/W]$, where the width W (assumed to be the same for all j) is treated as a fitting parameter. Such a calculation gives a profile which reproduces well the exact $p_{n,+}$, as shown in Fig. 7. This further confirms the picture that the edge state transfers to each extended state and then travels at its group velocity.

APPENDIX B: FIDELITY OF ADIABATIC TRANSFER

The power-law scalings we found occur when the state does not evolve to the other edge (the edges) of the chain;

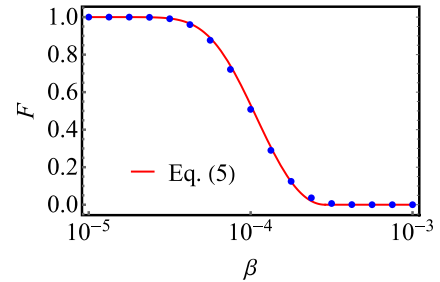


FIG. 8. Fidelity of adiabatic transfer in the SSH model, F vs β , for $N = 100$ for evolutions from an edge. The blue dots are exact results, and the red dashed line is Eq. (B1).

namely, we have effectively been considering a semi-infinite (infinite) chain. For a finite chain with an odd number of sites, in the adiabatic limit $\beta \rightarrow 0$ we expect that $|1, A\rangle$ evolves adiabatically to $|N, A\rangle$ since the edge state is always gapped from other states. For a larger β this adiabatic transfer is not perfect, and its efficiency can be characterized by the fidelity $F = |\langle N, B | \psi(t_f) \rangle|^2$. In Fig. 8 we plot F vs β for a chain with $N = 100$ with an odd number of sites. We found that F can be fitted by a simple formula:

$$F = \left[\max\left(1 - 2e^{-\frac{2}{N^2\beta}}, 0\right) \right]^2, \quad (\text{B1})$$

which works for different values of N . The appearance of $1 - 2e^{-2/(N^2\beta)}$ in (B1) reminds us the transition probability of staying on the middle level in the bow-tie model [68] and implies that the considered SSH model with linear time dependence may be somewhat similar to the bow-tie model.

-
- [1] C. H. Bennett and S. J. Wiesner, Communication via one- and two-particle operators on Einstein-Podolsky-Rosen states, *Phys. Rev. Lett.* **69**, 2881 (1992).
- [2] C. H. Bennett, G. Brassard, C. Crépeau, R. Jozsa, A. Peres, and W. K. Wootters, Teleporting an unknown quantum state via dual classical and Einstein-Podolsky-Rosen channels, *Phys. Rev. Lett.* **70**, 1895 (1993).
- [3] S. Bose, Quantum communication through an unmodulated spin chain, *Phys. Rev. Lett.* **91**, 207901 (2003).
- [4] M. Christandl, N. Datta, A. Ekert, and A. J. Landahl, Perfect state transfer in quantum spin networks, *Phys. Rev. Lett.* **92**, 187902 (2004).
- [5] M. Bellec, G. M. Nikolopoulos, and S. Tzortzakakis, Faithful communication Hamiltonian in photonic lattices, *Opt. Lett.* **37**, 4504 (2012).
- [6] A. Perez-Leija, R. Keil, A. Kay, H. Moya-Cessa, S. Nolte, L. C. Kwek, B. M. Rodríguez-Lara, A. Szameit, and D. N. Christodoulides, Coherent quantum transport in photonic lattices, *Phys. Rev. A* **87**, 012309 (2013).
- [7] R. J. Chapman, M. Santandrea, Z. Huang, G. Corrielli, A. Crespi, M. H. Yung, R. Osellame, and A. Peruzzo, Experimental perfect state transfer of an entangled photonic qubit, *Nat. Commun.* **7**, 11339 (2016).
- [8] Y. X. Shen, Y. G. Peng, D. G. Zhao, X. C. Chen, J. Zhu, and X. F. Zhu, One-way localized adiabatic passage in an acoustic system, *Phys. Rev. Lett.* **122**, 094501 (2019).
- [9] N. Y. Yao, L. Jiang, A. V. Gorshkov, Z.-X. Gong, A. Zhai, L. M. Duan, and M. D. Lukin, Robust quantum state transfer in random unpolarized spin chains, *Phys. Rev. Lett.* **106**, 040505 (2011).
- [10] F. Mei, G. Chen, L. Tian, S. L. Zhu, and S. Jia, Robust quantum state transfer via topological edge states in superconducting qubit chains, *Phys. Rev. A* **98**, 012331 (2018).
- [11] D. I. Tsomokos, S. Ashhab, and F. Nori, Using superconducting qubit circuits to engineer exotic lattice systems, *Phys. Rev. A* **82**, 052311 (2010).
- [12] D. Petrosyan and P. Lambropoulos, Coherent population transfer in a chain of tunnel coupled quantum dots, *Opt. Commun.* **264**, 419 (2006).
- [13] Y. A. Chen, S. Nascimbène, M. Aidelsburger, M. Atala, S. Trotzky, and I. Bloch, Controlling correlated tunneling and superexchange interactions with ac-driven optical lattices, *Phys. Rev. Lett.* **107**, 210405 (2011).
- [14] P. Cappellaro, C. Ramanathan, and D. G. Cory, Simulations of information transport in spin chains, *Phys. Rev. Lett.* **99**, 250506 (2007).
- [15] S. Ashhab, P. C. de Groot, and F. Nori, Speed limits for quantum gates in multiqubit systems, *Phys. Rev. A* **85**, 052327 (2012).
- [16] T. Caneva, M. Murphy, T. Calarco, R. Fazio, S. Montangero, V. Giovannetti, and G. E. Santoro, Optimal control at the quantum speed limit, *Phys. Rev. Lett.* **103**, 240501 (2009).

- [17] S. Deffner and S. Campbell, Quantum speed limits: From Heisenberg's uncertainty principle to optimal quantum control, *J. Phys. A* **50**, 453001 (2017).
- [18] M. H. Yung, Quantum speed limit for perfect state transfer in one dimension, *Phys. Rev. A* **74**, 030303(R) (2006).
- [19] X. M. Zhang, Z. W. Cui, X. Wang, and M. H. Yung, Automatic spin-chain learning to explore the quantum speed limit, *Phys. Rev. A* **97**, 052333 (2018).
- [20] T. Graß, D. Raventós, B. Juliá-Díaz, G. Christian, and M. Lewenstein, Quantum annealing for the number-partitioning problem using a tunable spin glass of ions, *Nat. Commun.* **7**, 11524 (2016).
- [21] S. Knysh, Zero-temperature quantum annealing bottlenecks in the spin-glass phase, *Nat. Commun.* **7**, 12370 (2016).
- [22] R. Barends *et al.*, Digitized adiabatic quantum computing with a superconducting circuit, *Nature (London)* **534**, 222 (2016).
- [23] M. Z. Hasan and C. L. Kane, Colloquium: Topological insulators, *Rev. Mod. Phys.* **82**, 3045 (2010).
- [24] X. L. Qi and S. C. Zhang, Topological insulators and superconductors, *Rev. Mod. Phys.* **83**, 1057 (2011).
- [25] S. D. Das Sarma, M. Freedman, and C. Nayak, Topological quantum computation, *Phys. Today* **59**(7), 32 (2006).
- [26] B. Gardas, J. Dziarmaga, W. H. Zurek, and M. Zwolek, Defects in quantum computers, *Sci. Rep.* **8**, 4539 (2018).
- [27] M. P. Estarellas, I. D'Amico, and T. P. Spiller, Topologically protected localized states in spin chains, *Sci. Rep.* **7**, 42904 (2017).
- [28] N. Lang and H. P. Büchler, Topological networks for quantum communication between distant qubits, *npj Quantum Inf.* **3**, 47 (2017).
- [29] S. Longhi, Topological pumping of edge states via adiabatic passage, *Phys. Rev. B* **99**, 155150 (2019).
- [30] S. Longhi, G. L. Giorgi, and R. Zambrini, Landau Zener topological quantum state transfer, *Adv. Quantum Technol.* **2**, 1800090 (2019).
- [31] F. M. D'Angelis, F. A. Pinheiro, D. Guéry-Odelin, S. Longhi, and F. Impens, Fast and robust quantum state transfer in a topological Su-Schrieffer-Heeger chain with next-to-nearest-neighbor interactions, *Phys. Rev. Res.* **2**, 033475 (2020).
- [32] J. Xu, F. Mei, and Y.-Q. Zhu, A universal shortcut method for state transfer in quantum spin systems, *arXiv:2312.08920*.
- [33] A. Y. Kitaev, Unpaired Majorana fermions in quantum wires, *Phys. Usp.* **44**, 131 (2001).
- [34] J. K. Asbóth, L. Oroszlány, and A. Pályi, *A short course on topological insulators*, Lecture Notes in Physics Vol. 919 (Springer, Cham, 2016).
- [35] D. J. Thouless, Quantization of particle transport, *Phys. Rev. B* **27**, 6083 (1983).
- [36] T. W. B. Kibble, Topology of cosmic domains and strings, *J. Phys. A* **9**, 1387 (1976).
- [37] T. W. B. Kibble, Some implications of a cosmological phase transition, *Phys. Rep.* **67**, 183 (1980).
- [38] W. H. Zurek, Cosmological experiments in superfluid helium? *Nature (London)* **317**, 505 (1985).
- [39] W. H. Zurek, Cosmological experiments in condensed matter systems, *Phys. Rep.* **276**, 177 (1996).
- [40] M. Lee, S. Han, and M.-S. Choi, Kibble-Zurek mechanism in a topological phase transition, *Phys. Rev. B* **92**, 035117 (2015).
- [41] A. Jamadagni, J. Kazemi, and A. Bhattacharyya, Kibble-Zurek mechanism and errors of gapped quantum phases, *arXiv:2401.13625v2*.
- [42] S. Deuschländer, P. Dillmann, G. Maret, and P. Keim, Kibble-Zurek mechanism in colloidal monolayers, *Proc. Natl. Acad. Sci. USA* **112**, 6925 (2015).
- [43] S. Maegochi, K. Ienaga, and S. Okuma, Kibble-Zurek mechanism for dynamical ordering in a driven vortex system, *Phys. Rev. Lett.* **129**, 227001 (2022).
- [44] K. Du, X. Fang, C. Won, C. De, F. T. Huang, W. Xu, H. You, F. J. Gómez-Ruiz, A. del Campo, and S. W. Cheong, Kibble-Zurek mechanism of Ising domains, *Nat. Phys.* **19**, 1495 (2023).
- [45] C. N. Weiler, T. W. Neely, D. R. Scherer, A. S. Bradley, M. J. Davis, and B. P. Anderson, Spontaneous vortices in the formation of Bose-Einstein condensates, *Nature (London)* **455**, 948 (2008).
- [46] G. Lamporesi, S. Donadello, S. Serafini, F. Dalfovo, and G. Ferrari, Spontaneous creation of Kibble-Zurek solitons in a Bose-Einstein condensate, *Nat. Phys.* **9**, 656 (2013).
- [47] N. Navon, A. L. Gaunt, R. P. Smith, and Z. Hadzibabic, Critical dynamics of spontaneous symmetry breaking in a homogeneous Bose gas, *Science* **347**, 167 (2015).
- [48] M. Anquez, B. A. Robbins, H. M. Bharath, M. Boguslawski, T. M. Hoang, and M. S. Chapman, Quantum Kibble-Zurek mechanism in a spin-1 Bose-Einstein condensate, *Phys. Rev. Lett.* **116**, 155301 (2016).
- [49] B. Ko, J. W. Park, and Y. Shin, Kibble-Zurek universality in a strongly interacting Fermi superfluid, *Nat. Phys.* **15**, 1227 (2019).
- [50] C. R. Yi, S. Liu, R. H. Jiao, J. Y. Zhang, Y. S. Zhang, and S. Chen, Exploring inhomogeneous Kibble-Zurek mechanism in a spin-orbit coupled Bose-Einstein condensate, *Phys. Rev. Lett.* **125**, 260603 (2020).
- [51] A. Keesling, A. Omran, H. Levine, H. Bernien, H. Pichler, S. Choi, R. Samajdar, S. Schwartz, P. Silvi, S. Sachdev, P. Zoller, M. Endres, M. Greiner, V. Vuletić, and M. D. Lukin, Quantum Kibble-Zurek mechanism and critical dynamics on a programmable Rydberg simulator, *Nature (London)* **568**, 207 (2019).
- [52] S. Ebadi, T. T. Wang, H. Levine, A. Keesling, G. Semeghini, A. Omran, D. Bluvstein, R. Samajdar, H. Pichler, W. W. Ho, S. Choi, S. Sachdev, M. Greiner, V. Vuletić, and M. D. Lukin, Quantum phases of matter on a 256-atom programmable quantum simulator, *Nature (London)* **595**, 227 (2021).
- [53] A. del Campo, Universal statistics of topological defects formed in a quantum phase transition, *Phys. Rev. Lett.* **121**, 200601 (2018).
- [54] H.-B. Zeng, C.-Y. Xia, and A. del Campo, Universal breakdown of Kibble-Zurek scaling in fast quenches across a phase transition, *Phys. Rev. Lett.* **130**, 060402 (2023).
- [55] F. Balducci, M. Beau, J. Yang, A. Gambassi, and A. del Campo, Large deviations beyond the Kibble-Zurek mechanism, *Phys. Rev. Lett.* **131**, 230401 (2023).
- [56] M. Creutz, End states, ladder compounds, and domain-wall fermions, *Phys. Rev. Lett.* **83**, 2636 (1999).
- [57] R. Jafari, H. Johannesson, A. Langari, and M. A. Martin-Delgado, Quench dynamics and zero-energy modes: The case of the Creutz model, *Phys. Rev. B* **99**, 054302 (2019).
- [58] A. Coutant, V. Achilleos, O. Richoux, G. Theoharis, and V. Pagneux, Robustness of topological corner modes against

- disorder with application to acoustic networks, *Phys. Rev. B* **102**, 214204 (2020).
- [59] N. A. Sinitsyn, Exact results for models of multichannel quantum nonadiabatic transitions, *Phys. Rev. A* **90**, 062509 (2014).
- [60] N. A. Sinitsyn and F. Li, Solvable multistate model of Landau-Zener transitions in cavity QED, *Phys. Rev. A* **93**, 063859 (2016).
- [61] F. Li, C. Sun, V. Y. Chernyak, and N. A. Sinitsyn, Multistate Landau-Zener models with all levels crossing at one point, *Phys. Rev. A* **96**, 022107 (2017).
- [62] F. Li, V. Y. Chernyak, and N. A. Sinitsyn, Quantum annealing and thermalization: Insights from integrability, *Phys. Rev. Lett.* **121**, 190601 (2018).
- [63] L. Landau, Zur theorie der energieubertragung II, *Phys. Z. Sowjetunion* **2**, 46 (1932); C. Zener, Non-adiabatic crossing of energy levels, *Proc. R. Soc.* **137**, 696 (1932); E. Majorana, Atomi orientati in campo magnetico variabile, *Nuovo Cim.* **9**, 43 (1932); E. C. G. Stückelberg, Theorie der unelastischen Stösse zwischen Atomen, *Helv. Phys. Acta* **5**, 370 (1932).
- [64] We found that transition probabilities from the edge state to the two extended states at the same k with positive and negative energies are the same, which is due to the chiral symmetry. They are thus denoted by the same symbol, p_k .
- [65] One may think that a transition within a 2×2 bulk, namely, from $|\psi_{k,+}\rangle$ to $|\psi_{k,-}\rangle$, can take place, which may influence the estimate of d_{bulk} . Actually, at the wave vector k_{max} (whose value will be determined shortly) we will use to calculate $d_{T,\text{bulk}}$, such a transition can be ignored for the following reason. Each 2×2 block can be described by a two-state LZ model $H = 2\beta \sin(k/2)t\sigma_z + \cos(k/2)\sigma_x$, and the LZ model corresponding to the value of k_{max} is in the adiabatic region since $\exp(-2\pi\Gamma) = \exp[-2\pi \cos^2(k_{\text{max}}/2)/\{4\beta \sin(k_{\text{max}}/2)\}] \ll 1$ in the whole range of β considered, so transition amplitudes between $|\psi_{k,+}\rangle$ and $|\psi_{k,-}\rangle$ are vanishingly small.
- [66] As argued in [65], when considering $p_{n,+}$ near the peak, evolutions of all $|k\rangle \otimes |\psi_{k,+}\rangle$ states involved can be treated as adiabatic.
- [67] S. N. Shevchenko, S. Ashhab, and F. Nori, Landau-Zener-Stueckelberg interferometry, *Phys. Rep.* **492**, 1 (2010).
- [68] V. N. Ostrovsky and H. Nakamura, Exact analytical solution of the N -level Landau-Zener-type bow-tie model, *J. Phys. A* **30**, 6939 (1997).